Applied Catalysis B: Environmental 209 (2017) 483–492

Contents lists available at ScienceDirect

Applied Catalysis B: Environmental

journal homepage: www.elsevier.com/locate/apcatb

Photocatalytic valorization of glycerol to hydrogen: Optimization of operating parameters by artificial neural network

M.R. Karimi Estahbanati [a], Mehrzad Feilizadeh [b], Maria C. Iliuta [a,*]

[a] Department of Chemical Engineering, 1065 Av. De la Médecine, Université Laval, Québec, Québec G1V 0A6, Canada
[b] School of Chemical and Petroleum Engineering, Shiraz University, Shiraz, Iran

ARTICLE INFO

Article history:
Received 24 December 2016
Received in revised form 1 March 2017
Accepted 2 March 2017
Available online 4 March 2017

Keywords:
Hydrogen
Photocatalysis
Glycerol
Artificial neural network
Optimization

ABSTRACT

Glycerol is a considerable by-product of biodiesel production from biomass. Photocatalytic glycerol valorization to hydrogen is an attractive approach from the sustainable development point of view. This study investigates the individual and interaction effects of main operating parameters of the photocatalytic hydrogen production process from glycerol using Pt/TiO_2 photocatalyst. Four key operating parameters (i.e. glycerol%, catalyst loading, Pt% and pH) were selected as independent variables, and the amount of produced hydrogen was considered as the dependent variable (response). Experiments were conducted based on the Box-Behnken design. Response surface methodology (RSM) and Artificial Neural Network (ANN) models were developed based on the experimental design approach to predict hydrogen production. The predictive capacity of the two models was compared based on R^2, R^2_{adj}, *RMS*, *MAE* and *AAD*. The ANN model was found more accurate and reliable, and it was therefore employed for the optimization of H_2 production and parametric investigation. Analysis of the results showed that the operating parameters can also influence each other's optimum value. Increasing glycerol% shifts the optimum values of catalyst loading, Pt%, and pH to higher values; however, Pt% has a negligible effect on the optimum values of the other parameters. Moreover, the catalyst loading and pH have no effect on the optimum value of glycerol%, but the increase of each of these two parameters reduces the optimum value of glycerol% and Pt%. The Genetic Algorithm along with the ANN model was also utilized for the optimization and it was found that the overall optimum of the system was 50% glycerol (v/v), 3.9 g/L catalyst loading, 3.1% Pt, and pH 4.5. Finally, Garson's method was employed to obtain the relative importance of each variable in the system. This analysis revealed that the variation of glycerol% and catalyst loading had, respectively, the least and the most effect on the amount of produced hydrogen.

1. Introduction

In recent years, global energy crises have led to the development of renewable energies like biodiesel and hydrogen [1]. Due to abundance of water on earth, water splitting using solar light driven photocatalysts is a promising alternative for future energy production. Despite vast research in this area, still more studies are required to increase the efficiency of the photocatalysis process. One the other hand, the price of glycerol, one of the biodiesel byproducts, has decreased significantly due to overproduction [2]. Valorization of sustainable glycerol to green fuels is therefore another promising alternative for future energy production. In addition, investigation of glycerol photo-reforming can assist with clarifying the mechanisms of photocatalysis. This knowledge is also beneficial to increase insight into water photo-splitting as well as glycerol photo-conversion to valuable liquid products.

TiO_2 is the most common photocatalyst which benefits from advantages like very high photocatalyst activity, low cost, suitable chemical and thermal stability, and low toxicity [3,4]. These advantages make TiO_2 a promising photocatalyst; however, more research is required to achieve an economically viable hydrogen production process on an industrial scale. One of the most efficient techniques to increase the photocatalytic activity of TiO_2 is incorporating metals or metal oxides as co-catalysts [5]. The presence of co-catalysts could provide hydrogen reaction sites, favor the charge separation reaction, trap photo-generated electrons and extend light absorption toward the visible range [6].

* Corresponding author.
E-mail address: maria-cornelia.iliuta@gch.ulaval.ca (M.C. Iliuta).

http://dx.doi.org/10.1016/j.apcatb.2017.03.016
0926-3373/

Table 1
Experimental ranges and levels of variables for hydrogen production experiments.

Variables	−1	0	+1
Glycerol% (A, v/v)	0.5	25.25	50
Catalyst loading (B, g/L)	0.05	2.525	5
Pt% (C, wt%)	0.02	2.51	5
Initial pH of solution (D)	2	7	12

Among the metals used as co-catalysts in the photocatalytic glycerol conversion to hydrogen, like Pt [7–21], Cu [16,20,22–31], Au [12,13,21,32–34], Pd [12,13,21,35], Ni [21,30,36,37], Co [21,38], Ag [21,39], Mn [21], Cr [21], and W [21], Pt is the one most commonly used. Fu et al. [40] found that Pt decorated photocatalysts exhibited the highest hydrogen production rate and the photocatalytic activity decreased in the order of Pt > Au > Pd > Rh > Ag > Ru. In another work, Pt was found to be the most active co-catalyst for hydrogen production by investigating the vast range of Pt, Pd, Ir, Au, Ru, Rh, and Ni [41]. Recently, López-Tenllado et al. [13] reported the order of Pt > Pd > Au for propan-2-ol and Pt ≈ Au > Pd for glycerol photocatalytic valorization to hydrogen.

Although there is much research on the synthesis of photocatalyst and feasibility of hydrogen production from glycerol, this field suffers from the lack of optimization of operating parameters. On the other hand, it is very challenging to develop a consensus on the optimum value of operating parameters due to significant differences and contradictions in previous work [42]. These conflicts may be attributed to the application of a 'one-variable-at-a-time' approach and to a disregard for the interaction effect of the parameters [43].

To assess the interaction effect of various operating parameters, a comprehensive model is required. Response Surface Methodology (RSM) and Artificial Neural Networks (ANN) are two useful modeling methods that can be applied for complex processes like photocatalytic hydrogen production because they do not require knowledge about the fundamentals of the photocatalytic process [44]. RSM is a statistical method to design experiments, develop a model, investigate effects of parameters, assess the interaction effect of the parameters, and optimize the desired responses [45,46]. ANN was inspired by biological neural networks taking advantage of some simple and non-linear models [47]. The Genetic Algorithm (GA) can be further employed to optimize the output of ANN models. GA utilizes a robust optimization procedure that mimics the process of natural selection, and its global optimizing capability is more powerful in comparison with other heuristic optimization methods [48].

To the best of our knowledge, a single statistical analysis on glycerol conversion to hydrogen has been reported to date. Bastos et al. [49] examined the glycerol valorization to hydrogen using a simple factorial design statistical model. The critical point which was obtained corresponded to a minimum, i.e., no optimization could be performed using this model. On the other hand, there is no publication in this field using other powerful methods such as RSM or ANN. Moreover, no statistical analysis study was found on the optimization of glycerol valorization to hydrogen using a TiO_2 based photocatalyst (as the most common photocatalyst).

Herein, we investigated individual and interaction effects of four key operating parameters (including catalyst loading, Pt%, glycerol%, and pH) on the photocatalytic glycerol valorization to hydrogen rate using Pt/TiO_2. Two approaches of RSM and ANN were employed to model the process, and their predictive ability for photocatalytic hydrogen production reactions was compared. Moreover, GA was applied to optimize the response of the ANN model. Finally, the level of influence of each operating parameter on the amount of produced hydrogen was calculated.

2. Materials and methods

2.1. Materials

The commercial TiO_2 Aeroxide P25 (≥99.5%) photocatalyst was provided by Evonik Industries. Hexachloroplatinic acid (IV) ($H_2PtCl_6{\cdot}6H_2O$, ≥37.50% Pt) was obtained from Sigma–Aldrich to be used as the platinum precursor. Glycerol (≥99.5%) and ethyl alcohol (99.99%) were supplied by Caledon and Commercial Alcohols, respectively. pH adjustment was made using NaOH (≥97%) and HCl (36.5–38.0%) which were purchased from VWR. Milli-Q water was utilized in the synthesis of photocatalysts.

2.2. Preparation of Pt/TiO_2 photocatalyst

Platinum deposition on TiO_2 was performed based on the photodeposition method [18]. Briefly, a suspension of 1 g TiO_2 and 120 ml ethyl alcohol solution (10%) was sonicated for 30 min using a Hielscher UP400S Ultrasonic Processor. Hexachloroplatinic acid solution in water was then added to the suspension in order to obtain Pt loadings of 0.02, 2.51, and 5 wt%. The mixture was purged with nitrogen for 15 min to remove the oxygen present in the mixture. A photoreactor equipped with four 20 W Black-Ray® mercury tubes (365 nm) was used to perform the photocatalytic experiments. The irradiation was maintained for 3 h under continued nitrogen flow and constant 500 rpm magnetic stirring in all experiments. Finally, the Pt/TiO_2 material was filtered, washed and dried overnight at 110 °C.

2.3. Photocatalyst characterization

Powder X-ray diffraction (XRD) patterns of the prepared samples were obtained using a Bruker SMART APEXII X-ray diffractometer equipped with Cu Kα radiation source (λ = 1.5418 Å). The patterns were measured from 2θ = 10–80° at a step of 0.02° and a scan rate of 1.2 min^{-1}. The Anatase:Rutile ratio of the samples was calculated using Eq. (1) [50]:

$$\%Rutile = \frac{1}{\left[1 + 0.8(I_A/I_B)\right]} \times 100 \quad (1)$$

where I_A and I_B are, respectively, the intensities of anatase (101) and rutile (110) reflections. TEM images were collected using a JOEL JEM 1230 operated an accelerating voltage of 120 kV. To prepare the samples for the analysis, they were dispersed in water and sonicated using a Hielscher UP400S Ultrasonic Processor and then placed on carbon coated copper TEM grids.

2.4. Hydrogen production experiments

The photocatalytic hydrogen production experiments were carried out in gas-tight Pyrex reaction cells using the prepared photocatalysts. In each experiment, predetermined amounts of glycerol, water, and photocatalyst (Table 2) were introduced into the cells. After sonication of the suspensions for 5 min to ensure proper dispersion of photocatalysts, the pH was adjusted using NaOH and HCl solutions. The volume of suspensions was ensured to be kept at 5 ml. Before irradiation, the reaction cells were purged with nitrogen (20 ml/min) for 15 min to remove oxygen and stirred in the dark for 20 min to allow the adsorption of glycerol on the catalyst surface. The cells were then irradiated with a light intensity of 1600 μW/cm^2 in a photoreactor equipped with four 20 W Black-Ray® mercury tubes. The spectral chart of the mercury tubes is illustrated in Fig. S1. During the experiments, the mixtures were maintained at constant 500 rpm magnetic stirring using Thermo-Scientific™ Cimarec™ 15-Position magnetic stirrer. The

Table 2
The box-behnken design of experiment along with actual and predicted values of the produced hydrogen.

Run #	Independent variables				Produced hydrogen[a]								
					Experimental			ANN			RSM		
	Glycerol% (v/v)	Catalyst loading (g/l)	Pt% (wt%)	pH	Yield	μmol g^{-1} h^{-1}	μmol	Yield	μmol g^{-1} h^{-1}	μmol	Yield	μmol g^{-1} h^{-1}	μmol
1	0.50	2.525	2.51	2	0.4211	2851	144	0.4385	2970	150	0.4327	2931	148
2	0.50	2.525	0.02	7	0.3625	2455	124	0.3654	2475	125	0.3567	2416	122
3	0.50	0.050	2.51	7	0.0819	28000	28	0.0409	14000	14	0.0906	31000	31
4	0.50	5.000	2.51	7	0.6169	2110	211	0.6139	2100	210	0.5584	1910	191
5	0.50	2.525	5.00	7	0.5321	3604	182	0.5496	3723	188	0.4707	3188	161
6	0.50	2.525	2.51	12	0.1666	1129	57	0.1841	1248	63	0.2719	1842	93
7	25.25	2.525	0.02	2	0.0060	2040	103	0.0059	2040	103	0.0066	2257	114
8	25.25	0.050	2.51	2	0.0014	25000	25	0.0012	22000	22	0.0015	26000	26
9	25.25	5.000	2.51	2	0.0156	2690	269	0.0151	2610	261	0.0155	2670	267
10	25.25	2.525	5.00	2	0.0133	4554	230	0.0134	4594	232	0.0138	4733	239
11	25.25	0.050	0.02	7	0.0016	28000	28	0.0017	30000	30	0.0005	10000	10
12	25.25	5.000	0.02	7	0.0084	1450	145	0.0085	1480	148	0.0088	1530	153
13	25.25	2.525	2.51	7	0.0148	5050	255	0.0145	4970	251	0.0143	4891	247
14	25.25	2.525	2.51	7	0.0143	4891	247	0.0145	4970	251	0.0143	4891	247
15	25.25	2.525	2.51	7	0.0146	5010	253	0.0145	4970	251	0.0143	4891	247
16	25.25	2.525	2.51	7	0.0137	4693	237	0.0145	4970	251	0.0143	4891	247
17	25.25	2.525	2.51	7	0.0141	4812	243	0.0145	4970	251	0.0143	4891	247
18	25.25	0.050	5.00	7	0.0032	56000	56	0.0034	60000	60	0.0034	60000	60
19	25.25	5.000	5.00	7	0.0141	2430	243	0.0143	2480	248	0.0158	2730	273
20	25.25	2.525	0.02	12	0.0043	1485	75	0.0034	1188	60	0.0039	1347	68
21	25.25	0.050	2.51	12	0.0008	14000	14	0.0009	17000	17	0.0001	2000	2
22	25.25	5.000	2.51	12	0.0076	1320	132	0.0076	1320	132	0.0068	1170	117
23	25.25	2.525	5.00	12	0.0071	2416	122	0.0067	2317	117	0.0064	2218	112
24	50.00	2.525	2.51	2	0.0075	5050	255	0.0074	5030	254	0.0068	4594	232
25	50.00	2.525	0.02	7	0.0035	2396	121	0.0033	2297	116	0.0037	2535	128
26	50.00	0.050	2.51	7	0.0013	44000	44	0.0019	67000	67	0.0019	65000	65
27	50.00	5.000	2.51	7	0.0077	2630	263	0.0077	2640	264	0.0076	2610	261
28	50.00	2.525	5.00	7	0.0081	5386	272	0.0077	5228	264	0.0076	5149	260
29	50.00	2.525	2.51	12	0.0031	2079	105	0.0025	1723	87	0.0033	2257	114

[a] Amount of hydrogen in 3.5 ml of gas headspace after 4 h.

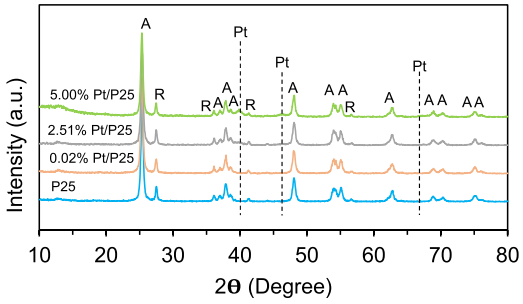

Fig. 1. XRD patterns of the photocatalyst samples with different platinum loadings.

temperature of the reactor was maintained around ambient (25 °C) using a cooling fan. The photocatalytic reactions were assessed after illumination of the samples for 4 h. To measure the amount of produced hydrogen in the photocatalytic reactions, 0.5 ml of gas headspace was sampled from the cells using a gas tight syringe with valve and injected to a Hewlett Packard HP 5890 gas chromatograph (GC) equipped with TCD detector, carboxen-1010 capillary column, and nitrogen carrier gas. Three replicate runs were performed to ensure the accuracy of the results. To ensure that no hydrogen was produced in the absence of illumination, a sample was also analyzed without the use of UV irradiation.

2.5. Design and analysis of experiments

2.5.1. Box-Behnken experimental design

The Box-Behnken experimental design was employed for the design of the experiment to evaluate the effect of four operating parameters, i.e., glycerol% (v/v%), catalyst loading (g/L), Pt% (wt%) and pH, which are respectively labeled A to D. These selected parameters were considered as the independent variables and the amount of produced hydrogen (μmol) after 4 h of irradiation was selected as the dependent variable (response). The experimental ranges were obtained based on preliminary experiments, as presented in Table 1. Accordingly, 29 sets of tests (including five center points) were defined for these four independent variables in three levels (coded as −1, 0, +1), as shown in Table 2. These data sets were then used to develop the RSM and ANN models.

2.5.2. RSM model

For RSM, a second-order polynomial equation (Eq. (2)) was obtained to model the amount of produced hydrogen as a function of the four independent variables mentioned above (A–D).

$$Y = \beta_0 + \beta_1 A + \beta_2 B + \beta_3 C + \beta_4 D + \beta_{12} AB + \beta_{13} AC + \beta_{14} AD + \beta_{23} BC + \beta_{24} BD + \beta_{34} CD + \beta_{11} A^2 + \beta_{22} B^2 + \beta_{33} C^2 + \beta_{44} D^2 \quad (2)$$

where Y is the amount of produced hydrogen (response), β_0 represents the interception coefficient, β_1, β_2, β_3, and β_4 are the coefficients of the independent variables, β_{11}, β_{22}, β_{33}, and β_{44} are the quadratic terms, and β_{12}, β_{13}, β_{14}, β_{23}, β_{24}, and β_{34} are the interaction coefficients [51]. Moreover, the analysis of variance (ANOVA) and optimization of produced hydrogen in the reaction were performed by Design-Expert® software (10.0.2.0 Stat-Ease, Inc. Minneapolis, USA).

2.5.3. ANN model

For ANN, a three-layer feed-forward neural network was developed and trained by back-propagation gradient-descendent algorithm. The obtained experimental data were randomly classified into three sets containing 23, 3, and 3 data to be employed for

train, test and validation, respectively. Training data sets were used for updating weights and biases via Levenberg–Marquardt algorithm and the test data were utilized to evaluate the generalization ability of the trained network. Moreover, the error of validation data was supervised during training to avoid overfitting [52]. A hyperbolic tangent sigmoid function and two linear functions were used as transfer functions for the neurons in the hidden layer and the neurons in the input and output layers, respectively. The input and output layers had 4 and 1 neurons, respectively. To determine the optimal number of neurons in the hidden layer, different topologies were examined during which the number of neurons varied between 2 and 10. Each topology was repeated 10 times to prevent random correlation because of random initialization of the weights and biases [53].

To evaluate the performance of the networks, the coefficient of determination (R^2), adjusted coefficient of determination (R^2_{adj}), root mean squared error (*RMS*), mean absolute error (*MAE*) and absolute average deviation (*AAD*) were calculated based on Eqs. (3)–(7). These parameters were also utilized to compare RSM and ANN models.

$$R^2 = 1 - \sum_{i=1}^{n} \left(\frac{(y_{i,cal} - y_{i,\exp})^2}{(y_{ave,\exp} - y_{i,\exp})^2} \right) \tag{3}$$

$$R^2_{adj} = 1 - \left[(1 - R^2) \frac{n-1}{n-K-1} \right] \tag{4}$$

$$RMS = \sqrt{\frac{\sum_{i=1}^{n} \left(X_{i,cal} - X_{i,\exp} \right)^2}{n}} \tag{5}$$

$$MAE = \frac{\sum_{i=1}^{n} |X_{i,cal} - X_{i,\exp}|}{n} \tag{6}$$

$$AAD = \left\{ \frac{\sum_{i=1}^{n} \left(|X_{i,cal} - X_{i,\exp}| / X_{i,cal} \right)}{n} \right\} \times 100 \tag{7}$$

where n represents the number of data points, K is the number of input variables, $X_{i,cal}$, $X_{i,\exp}$, and $X_{ave,\exp}$ are the response of predicted, experimental and arithmetic mean of all experimental data, respectively.

2.5.4. Genetic algorithm

GA optimization procedure was employed to optimize the ANN model. A primary population of 50 individuals with uniform distribution was randomly created to initialize the optimization procedure. A stochastic universal sampling was used as selection function, and the rank function was employed as fitness scaling function. In each generation, 80% and 15% of individuals were produced from crossover and mutation of the previous generation, respectively, and 5% of the population was chosen as elites and was guaranteed to survive to the next generation. Gaussian and scattered functions were used as the mutation and crossover functions respectively.

Table 3
Characteristics of the prepared photocatalyst samples.

Photocatalyst	Anatase crystal size (nm)	Rutile crystal size (nm)	Rutile fraction (wt%)
P25	20	31	16
2.51% Pt/P25	19	30	17
5% Pt/P25	20	33	18
0.02% Pt/P25	20	28	16

2.5.5. Garson's method

Garson's method was employed to obtain the level of influence of variables on the response. This method is based on Eq. (8) which uses the connection weights of the neural network [54,55]:

$$I_j = \frac{\sum_{m=1}^{m=N_h} \left(\left(|W^{ih}_{jm}| / \sum_{k=1}^{k=N_i} |W^{ih}_{km}| \right) \times |W^{ho}_{mn}| \right)}{\sum_{k=1}^{k=N_i} \left\{ \sum_{m=1}^{m=N_h} \left(\left(|W^{ih}_{km}| / \sum_{k=1}^{k=N_i} |W^{ih}_{km}| \right) \times |W^{ho}_{mn}| \right) \right\}} \tag{8}$$

where I_j refers to the relative importance of the j^{th} input variable on the response, W represents the connection weights, and N_i and N_h refer to the numbers of input and hidden neurons, respectively. The superscripts '*i*', '*h*' and '*o*' denote input, hidden and output layers, and the subscripts '*k*', '*m*' and '*n*' are related to input, hidden and output neurons, respectively.

3. Results and discussion

3.1. Characterization of the prepared samples

XRD patterns of the prepared samples with different platinum loadings are presented in Fig. 1. It demonstrates that in all TiO_2 samples, the peaks related to Anatase and Rutile phases of TiO_2 remained intact after platinum deposition. Pt (111) reflection at $2\theta = 39.84^\circ$, which is characteristic of the face-centered cubic (fcc) structure of platinum [56], obviously grew at 5% of Pt. Regarding the Pt (200) and Pt (220) reflections at $2\theta = 46.32^\circ$ and 67.54°, only a slight shoulder can be observed for the sample loaded with 5% Pt [57]. Table 3 presents some characteristics for the prepared samples. The Scherrer equation [58] was employed to estimate the average Anatase (101) and Rutile (110) particle sizes which were found to be ca. 20 and 30 nm for all particles, respectively. The Anatase:Rutile ratio in TiO_2 was calculated based on the peak heights of Anatase (101) and Rutile (110) reflections [50], and was 1:6 for all of prepared samples. Similar particle sizes and phase ratios of TiO_2 particles confirm that the Pt photo-deposition process did not affect the size and crystal structure of the TiO_2 samples.

The morphology of the prepared sample was studied, and the deposition of platinum particles on TiO_2 was checked by TEM. Fig. 2 clearly displays deposited Pt particles on TiO_2 as black dots for the 5.00% Pt/P25 sample. Based on this figure, the average size of the particles was around 25 nm, and the mean metal nanoparticle size was around 2 nm, which is in the range of previous studies [11,12,15].

3.2. Experimental hydrogen production results

29 sets of experiments were performed based on Box-Behnken design to study the effect of the four operating parameters mentioned above on the amount of produced hydrogen. For this purpose, the range of glycerol% (v/v%), catalyst loading (g/L), Pt% (wt%) and pH were 0.5–50%, 0.05–5 g/L, 0.02–5%, and 2–12. The experimental design and obtained results are summerized in Table 2. These experimental data were utilized to implement the RSM and ANN models.

The yield of produced hydrogen after 4 h of experiments was calculated based on Eq. (9) and the results are presented in Table 2.

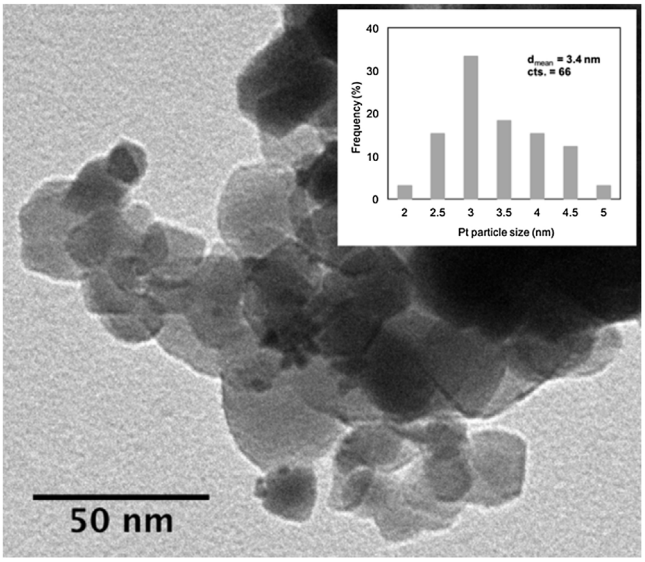

Fig. 2. TEM images of 5.00% Pt/P25 photocatalyst sample.

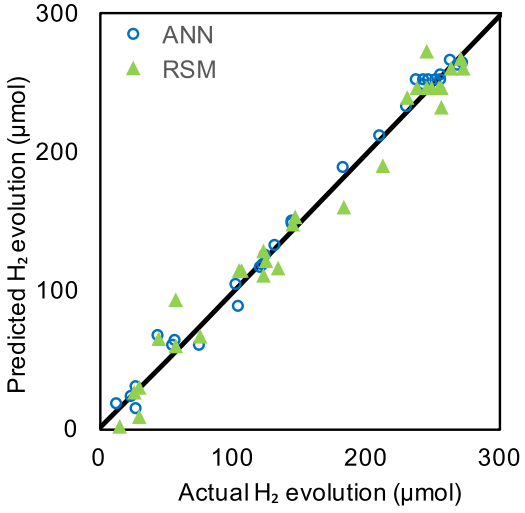

Fig. 3. The actual amount of produced hydrogen versus the predicted values by ANN and RSM models.

As can be seen, the yield is greater at lower initial glycerol concentrations and among the designed experiments, the maximum yield (0.6169) corresponds to catalyst loading = 5 g/L, Pt% = 2.51, glycerol% = 0.5 and pH = 7.

$$Yield = \frac{\mu mol\ \ produced\ \ H_2}{\mu mol\ \ glycerol\ \ fed} \quad (9)$$

3.3. Modeling

3.3.1. ANN model

Several networks with a different number of neurons in the hidden layer were evaluated to find the best configuration based on the minimum *RMS*. The neural network including a hidden layer with four neurons (architecture of 4-4-1) was found to be the most appropriate network structure to model the photocatalytic process. The predictions of the amount of produced hydrogen by the ANN model are listed in Table 2. The representation of predicted values versus experimental data (Fig. 3) shows a good predictive ability of the current ANN model. As seen in Table 4, the R^2 value of 0.9913 for the ANN model is in good agreement with the adjusted R^2_{adj} of 0.9800. The high value of R^2 denotes that the current ANN model is suitable for the prediction of this system. Furthermore, the small values of *RMS* (8.1706), *MAE* (5.9310) and *AAD* (8.1147) demonstrate that the developed ANN model has good approximation and generalization characteristics.

Table 4
Comparison of the predictive capacity of ANN and RSM models.

Parameter	RSM	ANN
R^2	0.9748	0.9913
$R^2_{adj.}$	0.9419	0.9800
RMS	13.9692	8.1706
AAD	14.1436	8.1147
MAE	10.8621	5.9310

3.3.2. RSM model

An empirical second-order polynomial equation was obtained based on RSM:

$$Y = -190 + 3.34A + 106B + 49.0C + 42.7D + 0.150AB + 0.377AC - 0.126AD + 2.86BC - 2.55BD - 1.61CD - 0.0540A^2 - 12.5B^2 - 7.46C^2 - 2.69D^2 \quad (10)$$

where Y represents the amount of produced hydrogen (μmol) and A, B, C, and D are, respectively, glycerol% (v/v%), catalyst loading (g/L), Pt% (wt%), and pH. The predicted values of produced hydrogen based on the current RSM model are presented in Table 2. The R^2, adjusted R^2_{adj}, *RMS*, *MAE*, and *AAD* of the developed RSM model which are presented in Table 4, show good approximation and generalization characteristics for this model. To find the combination accuracy of the coefficients, the current model (Eq. (10)) was statistically investigated by ANOVA. This analysis showed that the p-value of the model is lower than 0.0001 which confirms that the model is adequate with more than 99% significance level. The predicted values by the developed RSM model are compared with the experimental data in Fig. 3. As can be seen, although the fitting capability of the RSM model is very good, it is not as suitable as the ANN model.

3.3.3. Comparison of ANN and RSM models

The predicted values obtained from the ANN and RSM models and the corresponding accuracies and prediction capabilities of these two models (based on the values of R^2, R^2_{adj}, *RMS*, *AAD*, and *MAE*) are given in Table 2 and Table 4, respectively. As it can be inferred, R^2 of ANN model is closer to 1 compared to RSM model and R^2_{adj} of ANN model is in closer agreement with the corresponding R^2. Furthermore, the value of *RMS* obtained for ANN is closer to zero compared to the RSM model. Moreover, *AAD* corresponding to ANN is around twice less compared to RSM. Table 4 suggests that both models are suitable to predict this photocatalytic system. However, the ANN model is superior for both data fitting and predictive performance. While RSM is limited by a second order polynomial, ANN is a more reliable modeling technique to represent the nonlinearities of this system. Thus, in the forthcoming subsections, the performance of the photocatalytic process is assessed based on the ANN model.

3.4. Effects and optimum of operating parameters

The response surface plots of the amount of produced hydrogen as functions of six pairs of the independent variables (i.e. glycerol%, catalyst loading, Pt%, and pH) are depicted in Fig. 4. In all the plots, the values of the two parameters that are not varied in each graph have been fixed at the average of their ranges. Thus, these six surface plots pass through the average point of the system (catalyst loading = 2.525 g/L, Pt% = 2.51, glycerol% = 25 and pH = 7), where the amount of produced hydrogen is around 251 μmol. To compare the

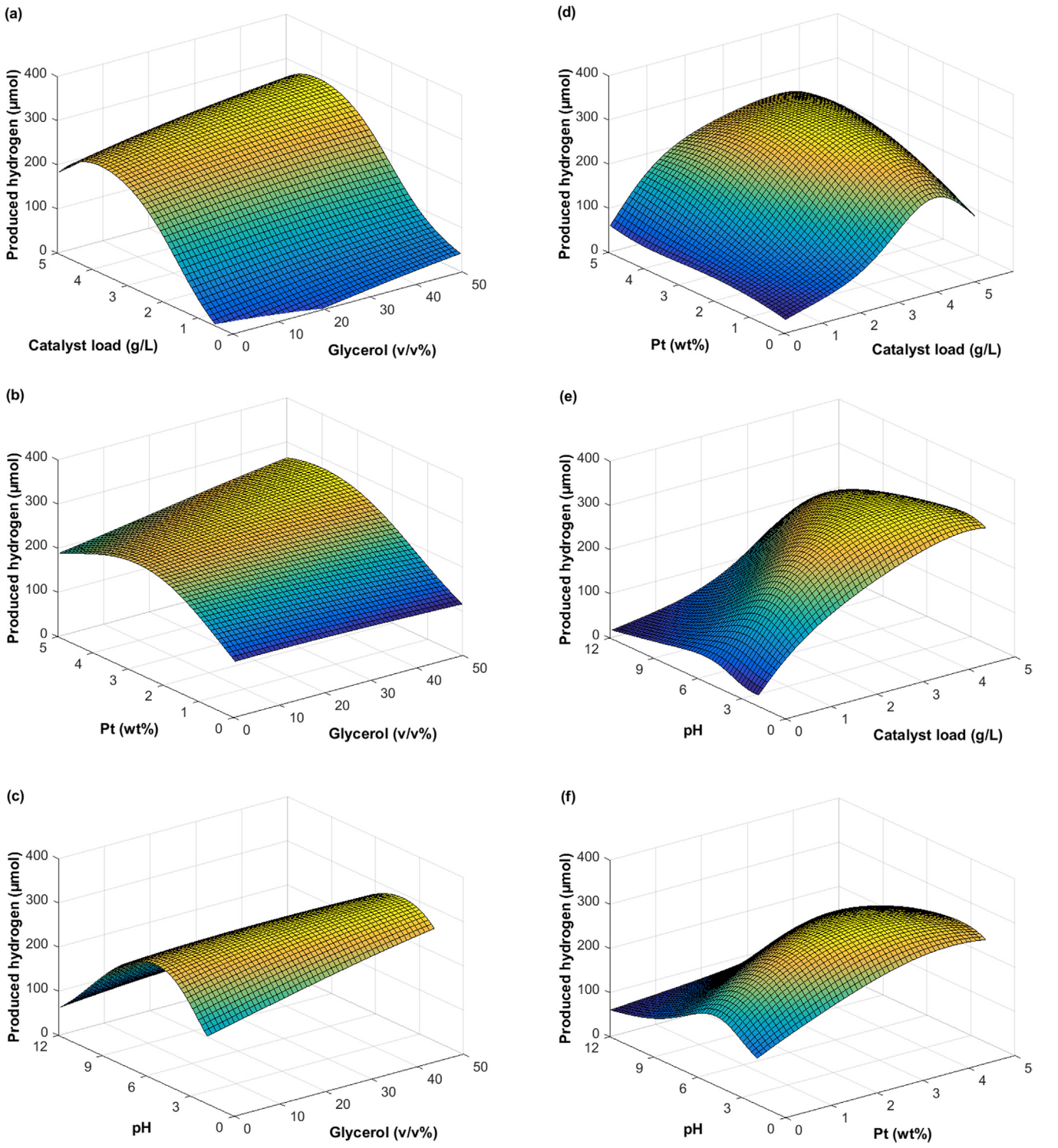

Fig. 4. Response surface plots of the amount of produced hydrogen as a function of (a) catalyst loading and glycerol%, (b) Pt% and glycerol%, (c) pH and glycerol%, (d) Pt and catalyst loading, (e) pH and catalyst loading, and (f) pH and Pt%. In all figures, the values of the two parameters not included in the graphs were considered equal to the average of their ranges.

interaction of operating parameters more easily and their influence on the optimum value of other parameters, the two-dimensional representations of the response surfaces of Fig. 4 are also shown in Figs. S2–S5. Similarly to Fig. 4, the two factors which are not presented in each of these four diagrams have been considered equal to the average of their ranges.

In the following subsections, the effects of the four operation parameters on the amount of produced hydrogen are discussed, as well as the effect of these parameters on the optimum value of other parameters.

3.4.1. Glycerol concentration

Fig. 4a–c illustrates that the amount of produced hydrogen is slightly enhanced by increasing glycerol%, even though the enhancement is not considerable, and increasing glycerol% from 0.5 to 50% enhances the amount of produced hydrogen to only around 61%. Improvement of the amount of produced hydrogen by increasing glycerol% can be due to easier access of the photocatalyst to the glycerol molecule [26].

Enhancement of the amount of produced hydrogen by increasing glycerol% agrees with existing literature. In the case of using Pt/TiO_2 for hydrogen production from glycerol, Daskalaki and Kondarides [7] reported that the amount of produced hydrogen was enhanced by increasing glycerol concentration from 0.073 to 7.93%. In another work conducted with the same photocatalyst but larger glycerol concentrations, it was found that the amount of produced hydrogen reached a plateau at high concentrations (up to 29.2%) [10]. Based on Fig. 4a–c, the optimum value of glycerol% is 50%, which can be considered in agreement with the 45% [17] and 53.6% [59] values reported as optimum glycerol% using TiO_2 photocatalyst.

Other than the amount of produced hydrogen, glycerol% could affect the optimum value of other parameters. According to Fig. 4a–c (and also Fig. S2), increasing glycerol% from 0.5 to 50% shifts the optimum catalyst loading from 3.75 to 3.95, the optimum Pt% from 2.75% to 4%, and the optimum pH from 4.4 to 6.4. By increasing glycerol%, the rate of oxidation half reaction increases, and further catalyst loading or Pt% provides more reaction sites for reduction half reaction.

3.4.2. Catalyst loading

The effect of catalyst loading on the amount of produced hydrogen can be seen in Fig. 4a, d, and e. Analysis of these surface plots reveals that the amount of produced hydrogen could be enhanced up to 8.1 times by the optimization of catalyst loading. Moreover, these surface plots show that catalyst loading around 4 g/L is optimal. Observation of an optimum value for catalyst loading may be due to the fact that, in a low amount of catalyst loading, a significant portion of radiated photons may transmit out of the photoreactor [60]. On the other hand, a high amount of catalyst loading may result in the tendency towards agglomeration of catalyst particles, thus rendering a part of the catalyst surface unavailable for photon absorption [61]. Other authors [7,38,62,63] have also reported an optimum value of catalyst loading in the photocatalytic hydrogen production reactions. The predictive accuracy of the developed model was compared to the experimental data given by Daskalaki and Kondarides [7], the only observed work in the literature on the investigation of hydrogen production from glycerol using Pt/TiO_2 with different catalyst loading. The evaluation of this research shows that in the experimental conditions (0.0027% of glycerol, 0.5% of Pt%, and pH of 7) given in [7], the optimum value of the catalyst loading that was predicted by the current ANN model is 2.7 g/L, which agrees very well with the reported optimum value of 2.7 g/L (based on their experimental data). This comparison confirms the accuracy of the developed model and its predictive ability in a wide range of parameters. It also suggests that the model based on ANN is a powerful tool for optimizing this kind of complex process.

Fig. 4a, d, and e, also represents the effect of catalyst loading on the optimum value of the other three independent variables (see Fig. S3 for more clarity). These figures imply that the catalyst loading has no effect on the optimum value of glycerol%, as the maximum amount of hydrogen is produced at 50% glycerol for all the catalyst loadings. However, by increasing the catalyst loading from 0.05 to 5 g/L, the optimum Pt% decreases from 5% to 3.9%. The reason for this observation could be due to the fact that at high catalyst loadings sufficient platinum particles are accessible to play the role of reaction site, and excessive Pt% makes a barrier against absorption of light by semiconductor and also prevents facile access of substrates to the semiconductor surface [64]. In addition, by increasing catalyst loading from 0.05 to 5 g/L, the optimum value of pH decreases from 5.7 to 3.5. This decrease could be attributed to supply of more reaction sites at higher catalyst loading, to convert higher concentration of hydronium ions (which are available at lower pH values) to hydrogen [65].

3.4.3. Pt%

It can be observed from Fig. 4b, d and f that hydrogen production hit a peak around 3–4% of platinum. The amount of produced hydrogen could increase up to 2.1 fold by the optimization of Pt%. As platinum plays the role of a photo-generated electron trap, it improves the charge separation of electron-hole and decreases the rate of recombination [66]. Thus, the amount of produced hydrogen is enhanced by increasing Pt% due to higher accessibility of platinum surface sites. Notwithstanding this, after the optimum point, addition of more platinum decreases the rate of photocatalytic reaction due to some issues such as light shielding and impeding access of substrate to semiconductor surface [64].

Observation of optimum values of co-catalyst agrees with previous research. For Pt-decorated TiO_2, optimum percentages of 2 [7] and 2.1 [67] were reported. In addition, in the case of using glycerol as hydrogen source, 1 [38], 2 [37] and 2.5 [24] percent of co-catalyst were obtained as optimum.

The influence of Pt% on the optimum value of the other three parameters could be discussed using Fig. 4b, d and f (see also Fig. S4). These figures suggest that Pt% has insignificant effects on the optimum values of glycerol%, catalyst loading, and pH which are around 50%, 4 g/L and 5, respectively.

3.4.4. pH

By analyzing Fig. 4c, d and f, it can be found that the amount of produced hydrogen could be enhanced up to 3.5 times by pH optimization. Moreover, these figures show that by changing pH from highly acidic solution to around 5, the amount of produced hydrogen increases; however, further growth of pH toward basic decreases the amount of produced hydrogen. Glycerol is adsorbed through hydrogen bonding with the surface hydroxyl groups of the photocatalyst (which are in the form of TiOH) [68]. The surface charge of the photocatalyst is neutral and glycerol could be adsorbed more conveniently around the point of zero charge (pH of 6.25 for P25 [10]). However, acidic solution causes agglomeration of P25 particles. On the other hand, in caustic solution, higher concentration of OH^- bonding leads to UV screening of photocatalyst [10]. Fig. 4c, d, and f, as well as Fig. S5 clarify the effect of pH on the optimum values of other operating parameters. Based on these figures, pH does not affect the optimum value of glycerol%. Conversely, decreasing pH from 12 to 5 shifts the optimum value of catalyst loading and Pt% respectively from 3.8 to 4.15 g/L and 3.1–5%. Variations of optimum catalyst loading and Pt% in different pH values could be attributed to the fact that a portion of surface active sites are not accessible in catalyst particles which agglomerate due to acidic pH [69]; thus, more catalyst loading or platinum is required to provide the necessary reaction sites. Furthermore, pH affects the electrokinetic potential of platinum particles and changes its capacity to trap photo-generated electrons and its adsorption of hydronium ions [65].

3.5. Overall optimization using GA

To find the maximum value of produced hydrogen and associated optimum operating parameters, the obtained ANN model was utilized as the fitness function in the optimization procedure based on GA. In the GA method, the population of the individual solutions was modified iteratively and the ANN model was employed

Table 5
The optimized value of hydrogen production and the four operating parameters based on GA.

Parameter	Produced hydrogen (μmol)		Glycerol% (v/v)	Catalyst loading (g/L)	Pt% (wt%)	pH
	Experimental	ANN model				
Optimized value	321	311	50	3.9	3.1	4.5

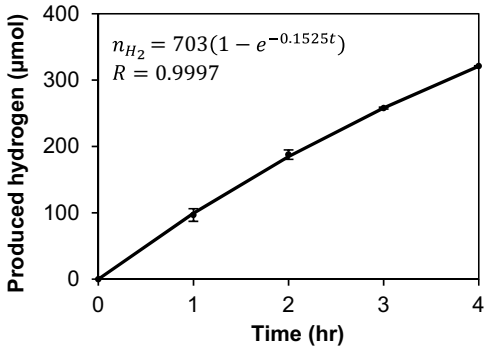

Fig. 5. The rate of produced hydrogen during 4 h at the optimum condition obtained by GA.

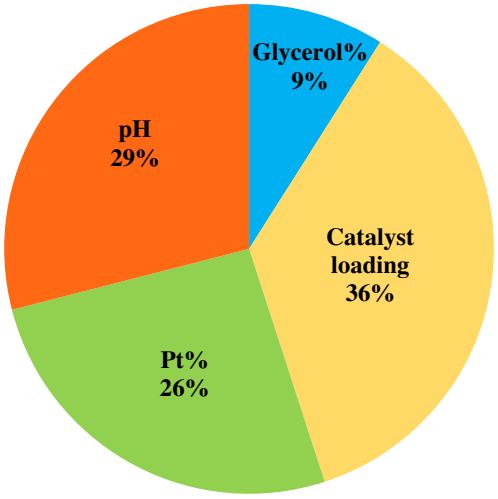

Fig. 6. The percentage relative importance of operating parameters in the current photocatalytic hydrogen production reaction.

to find the best generation in each iteration. Then the chosen generation was utilized to produce the next generation by reproduction, mutation and crossover (more detail about GA procedure can be found in [70]). The optimized values of hydrogen production and four operating parameters based on GA are summarized in Table 5. The optimum values of glycerol%, catalyst loading, Pt%, and pH were found to be respectively 50%, 3.9 g/L, 3.1%, and 4.5.

The ANN model predicted that 311 μmol of hydrogen will be produced in optimum conditions achieved by GA, which is very close to the 321 μmol obtained by experiments in these conditions and consequently, it confirms the accuracy of the model (see Table 5). Moreover, experimental data of the rate of produced hydrogen during 4 h in optimum conditions is represented in Fig. 5. As can be seen, the amount of produced hydrogen increased exponentially during the experiment.

3.6. Relative importance of the operating parameters

Garson's method (which uses the neural network weights matrix) was utilized to obtain the level of influence of each input variable on the response. Table S1 shows the connection weight values (neural network weights matrix) for the developed model. The relative importance of input variables computed by Eq. (8) is illustrated in Fig. 6. The results indicate that glycerol% and catalyst loading are, respectively, the least and most influential operating parameters with 9% and 36% effect on the amount of produced hydrogen. Moreover, the importance of Pt% and pH are approximately the same. This observation reveals that the amount of produced hydrogen is not significantly affected by the concentration of the glycerol, as this parameter does not control the reaction rate. On the other hand, the highest dependency of the amount of produced hydrogen to catalyst loading shows that the photocatalytic phenomenon is the main route for hydrogen production. This observation is in accordance with the 8.1 times enhancement of the amount of produced hydrogen by optimization of catalyst loading as represented in Fig. 4.

4. Conclusion

In this study, we investigated the interaction effects of key operating parameters in the photocatalytic glycerol valorization to hydrogen process using Pt/TiO_2 photocatalyst. Four operating parameters of glycerol%, catalyst loading, Pt%, and pH were selected as independent variables, and the value of produced hydrogen was considered as the response. The experiments were performed based on Box-Behnken experimental design. Two techniques of RSM and ANN were employed to model the process, and the obtained experimental data were utilized to train the models. Afterward, the optimization and predictive ability of these models were compared based on R^2, R^2_{adj}, *RMS*, *MAE* and *AAD*. This comparison revealed that the ANN-based model is more accurate and reliable; thus it was employed for the optimization and parametric investigation. Optimization of the ANN model was performed by the GA approach and it was found that the highest amount of hydrogen could be produced at the condition of 50% glycerol (v/v), 3.9 g/L catalyst loading, 3.1% Pt, and pH of 4.5. Garson's method was employed to obtain the relative importance of each operating parameter in the response. This analysis revealed that glycerol% and catalyst loading are, respectively, the least and most influential parameters on the amount of produced hydrogen. Moreover, analysis of the effect of operating parameters showed that, in addition to affecting the amount of produced hydrogen, they could affect the optimum values of other parameters.

Briefly, interaction effect analysis of the results showed that:

- Increasing glycerol% shifts the optimum value of catalyst loading, Pt% and pH to higher values.
- Catalyst loading has no effect on the optimum value of glycerol%; however, the optimum values of Pt% and pH decrease by increasing catalyst load.
- Pt% has insignificant effects on the optimum values of glycerol%, catalyst loading, and pH.
- pH does not affect the optimum value of glycerol%; however, decreasing pH shifts the optimum catalyst loading and Pt% to higher values.

Acknowledgements

The authors are very grateful to the Ministry of Education and Higher Education of Quebec, The Fonds de recherche du Québec – Nature et technologies (FRQNT), The Natural Sciences and Engineering Research Council of Canada (NSERC), TELUS, and Laval University for financial support and Ph.D. scholarships for M.R. Karimi Estahbanati.

Appendix A. Supplementary data

Supplementary data associated with this article can be found, in the online version, at http://dx.doi.org/10.1016/j.apcatb.2017.03.016.

References

[1] G. Corro, U. Pal, N. Tellez, Biodiesel production from Jatropha curcas crude oil using ZnO/SiO_2 photocatalyst for free fatty acids esterification, Appl. Catal. B: Environ. 129 (2013) 39–47.
[2] D. Sun, Y. Yamada, S. Sato, W. Ueda, Glycerol hydrogenolysis into useful C3 chemicals, Appl. Catal. B: Environ. 193 (2016) 75–92.
[3] M. Feilizadeh, M. Vossoughi, S.M.E. Zakeri, M. Rahimi, Enhancement of efficient Ag–S/TiO_2 nanophotocatalyst for photocatalytic degradation under visible light, Ind. Eng. Chem. Res. 53 (2014) 9578–9586.
[4] M. Feilizadeh, A. Delparish, S.T. Bararpour, H.A. Najafabadi, S.M.E. Zakeri, M. Vossoughi, Photocatalytic removal of 2-nitrophenol using silver and sulfur co-doped TiO_2 under natural solar light, Water Sci. Technol. 72 (2015) 339–346.
[5] M.R. Gholipour, C.-T. Dinh, F. Béland, T.-O. Do, Nanocomposite heterojunctions as sunlight-driven photocatalysts for hydrogen production from water splitting, Nanoscale 7 (2015) 8187–8208.
[6] L. Clarizia, D. Spasiano, I. Di Somma, R. Marotta, R. Andreozzi, D.D. Dionysiou, Copper modified-TiO2 catalysts for hydrogen generation through photoreforming of organics. A short review, Int. J. Hydrogen Energy 39 (2014) 16812–16831.
[7] V.M. Daskalaki, D.I. Kondarides, Efficient production of hydrogen by photo-induced reforming of glycerol at ambient conditions, Catal. Today 144 (2009) 75–80.
[8] N. Fu, G. Lu, Hydrogen evolution over heteropoly blue-sensitized Pt/TiO_2 under visible light irradiation, Catal. Lett. 127 (2008) 319–322.
[9] N. Fu, G. Lu, Photo-catalytic H2 evolution over a series of Keggin-structure heteropoly blue sensitized Pt/TiO2 under visible light irradiation, Appl. Surf. Sci. 255 (2009) 4378–4383.
[10] M. Li, Y. Li, S. Peng, G. Lu, S. Li, Photocatalytic hydrogen generation using glycerol wastewater over Pt/TiO_2, Front. Chem. China 4 (2009) 32–38.
[11] X. Fu, X. Wang, D.Y.C. Leung, Q. Gu, S. Chen, H. Huang, Photocatalytic reforming of C3-polyols for H_2 production: part (I). Role of their OH groups, Appl. Catal. B: Environ. 106 (2011) 681–688.
[12] Z.H.N. Al-Azri, W.-T. Chen, A. Chan, V. Jovic, T. Ina, H. Idriss, G.I.N. Waterhouse, The roles of metal co-catalysts and reaction media in photocatalytic hydrogen production: performance evaluation of M/TiO_2 photocatalysts (M = Pd, Pt, Au) in different alcohol-water mixtures, J. Catal. 329 (2015) 355–367.
[13] F.J. López-Tenllado, J. Hidalgo-Carrillo, V. Montes, A. Marinas, F.J. Urbano, J.M. Marinas, L. Ilieva, T. Tabakova, F. Reid, A comparative study of hydrogen photocatalytic production from glycerol and propan-2-ol on M/TiO_2 systems (M = Au, Pt, Pd), Catal. Today 280 (2017) 58–64.
[14] M.R. Pai, A.M. Banerjee, S.A. Rawool, A. Singhal, C. Nayak, S.H. Ehrman, A.K. Tripathi, S.R. Bharadwaj, A comprehensive study on sunlight driven photocatalytic hydrogen generation using low cost nanocrystalline Cu-Ti oxides, Sol. Energy Mater. Sol. Cells 154 (2016) 104–120.
[15] X. Jiang, X. Fu, L. Zhang, S. Meng, S. Chen, Photocatalytic reforming of glycerol for H_2 evolution on Pt/TiO_2: fundamental understanding the effect of co-catalyst Pt and the Pt deposition route, J. Mater. Chem. A 3 (2015) 2271–2282.
[16] D.W. Skaf, N.G. Natrin, K.C. Brodwater, C.R. Bongo, Comparison of photocatalytic hydrogen production from glycerol and crude glycerol obtained from biodiesel processing, Catal. Lett. 142 (2012) 1175–1179.
[17] Slamet, D. Tristantini, Valentina, M. Ibadurrohman, Photocatalytic hydrogen production from glycerol–water mixture over Pt-N-TiO_2 nanotube photocatalyst, Int. J. Energy Res. 37 (2013) 1372–1381.
[18] E.P. Melián, C.R. López, D.E. Santiago, R. Quesada-Cabrera, J.A.O. Méndez, J.M.D. Rodríguez, O.G. Díaz, Study of the photocatalytic activity of Pt-modified commercial TiO_2 for hydrogen production in the presence of common organic sacrificial agents, Appl. Catal. A: Gen. 518 (2016) 189–197.
[19] A. Beltram, I. Romero-Ocaña, J. Josè Delgado Jaen, T. Montini, P. Fornasiero, Photocatalytic valorization of ethanol and glycerol over TiO_2 polymorphs for sustainable hydrogen production, Appl. Catal. A: Gen. 518 (2016) 167–175.
[20] M. Jung, J.N. Hart, D. Boensch, J. Scott, Y.H. Ng, R. Amal, Hydrogen evolution via glycerol photoreforming over Cu–Pt nanoalloys on TiO_2, Appl. Catal. A: Gen. 518 (2016) 221–230.
[21] M. Stelmachowski, M. Marchwicka, E. Grabowska, M. Diak, A. Zaleska, The photocatalytic conversion of (Biodiesel derived) glycerol to hydrogen–a short review and preliminary experimental results part 2: photocatalytic conversion of glycerol to hydrogen in batch and semi-batch laboratory reactors, J. Adv. Oxid. Technol. 17 (2014) 179–186.
[22] D. Praveen Kumar, N. Lakshmana Reddy, M. Mamatha Kumari, B. Srinivas, V. Durga Kumari, B. Sreedhar, V. Roddatis, O. Bondarchuk, M. Karthik, B. Neppolian, M.V. Shankar, Cu_2O-sensitized TiO_2 nanorods with nanocavities for highly efficient photocatalytic hydrogen production under solar irradiation, Sol. Energy Mater. Sol. Cells 136 (2015) 157–166.
[23] T. Montini, V. Gombac, L. Sordelli, J.J. Delgado, X. Chen, G. Adami, P. Fornasiero, Nanostructured Cu/TiO_2 photocatalysts for H_2 production from ethanol and glycerol aqueous solutions, ChemCatChem 3 (2011) 574–577.
[24] K. Lalitha, G. Sadanandam, V.D. Kumari, M. Subrahmanyam, B. Sreedhar, N.Y. Hebalkar, Highly stabilized and finely dispersed Cu_2O/TiO_2: a promising visible sensitive photocatalyst for continuous production of hydrogen from glycerol:water mixtures, J. Phys. Chem. C 114 (2010) 22181–22189.
[25] V. Gombac, L. Sordelli, T. Montini, J.J. Delgado, A. Adamski, G. Adami, M. Cargnello, S. Bernal, P. Fornasiero, CuO_x-TiO_2 photocatalysts for H_2 production from ethanol and glycerol solutions, J. Phys. Chem. A 114 (2009) 3916–3925.
[26] A. Petala, E. Ioannidou, A. Georgaka, K. Bourikas, D.I. Kondarides, Hysteresis phenomena and rate fluctuations under conditions of glycerol photo-reforming reaction over CuO_x/TiO_2 catalysts, Appl. Catal. B: Environ. 178 (2015) 201–209.
[27] M. Zhang, R. Sun, Y. Li, Q. Shi, L. Xie, J. Chen, X. Xu, H. Shi, W. Zhao, High H_2 evolution from quantum Cu (II) nanodot-doped 2D ultrathin TiO_2 nanosheets with dominant exposed {001} facets for reforming glycerol with multiple electron transport pathways, J. Phys. Chem. C 120 (2016) 10746–10756.
[28] S.G. Babu, R. Vinoth, D.P. Kumar, M.V. Shankar, H.-L. Chou, K. Vinodgopal, B. Neppolian, Influence of electron storing, transferring and shuttling assets of reduced graphene oxide at the interfacial copper doped TiO_2 p-n heterojunction for increased hydrogen production, Nanoscale 7 (2015) 7849–7857.
[29] R. Bashiri, N.M. Mohamed, C.F. Kait, S. Sufian, Hydrogen production from water photosplitting using Cu/TiO_2 nanoparticles: effect of hydrolysis rate and reaction medium, Int. J. Hydrogen Energy 40 (2015) 6021–6037.
[30] F.K. Chong, E. Nurlaela, B.K. Dutta, Impact of glycerol as scavenger for solar hydrogen production from water, Int. J. Energy Environ. 8 (2014) 19–26.
[31] D.P. Kumar, M.V. Shankar, M.M. Kumari, G. Sadanandam, B. Srinivas, V. Durgakumari, Nano-size effects on CuO/TiO_2 catalysts for highly efficient H2 production under solar light irradiation, Chem. Commun. 49 (2013) 9443–9445.
[32] M. Bowker, P.R. Davies, L.S. Al-Mazroai, Photocatalytic reforming of glycerol over gold and palladium as an alternative fuel source, Catal. Lett. 128 (2008) 253–255.
[33] A.G. Dosado, W.-T. Chen, A. Chan, D. Sun-Waterhouse, G.I.N. Waterhouse, Novel Au/TiO_2 photocatalysts for hydrogen production in alcohol–water mixtures based on hydrogen titanate nanotube precursors, J. Catal. 330 (2015) 238–254.
[34] W.-T. Chen, A. Chan, Z.H.N. Al-Azri, A.G. Dosado, M.A. Nadeem, D. Sun-Waterhouse, H. Idriss, G.I.N. Waterhouse, Effect of TiO_2 polymorph and alcohol sacrificial agent on the activity of Au/TiO_2 photocatalysts for H_2 production in alcohol–water mixtures, J. Catal. 329 (2015) 499–513.
[35] H. Bahruji, M. Bowker, P.R. Davies, L.S. Al-Mazroai, A. Dickinson, J. Greaves, D. James, L. Millard, F. Pedrono, Sustainable H_2 gas production by photocatalysis, J. Photochem. Photobiol. A: Chem. 216 (2010) 115–118.
[36] R. Liu, H. Yoshida, S.-i. Fujita, M. Arai, Photocatalytic hydrogen production from glycerol and water with NiO_x/TiO_2 catalysts, Appl. Catal. B: Environ. 144 (2014) 41–45.
[37] S.-i. Fujita, H. Kawamori, D. Honda, H. Yoshida, M. Arai, Photocatalytic hydrogen production from aqueous glycerol solution using NiO/TiO_2 catalysts: effects of preparation and reaction conditions, Appl. Catal. B: Environ. 181 (2016) 818–824.
[38] G. Sadanandam, K. Lalitha, V.D. Kumari, M.V. Shankar, M. Subrahmanyam, Cobalt doped TiO_2: a stable and efficient photocatalyst for continuous hydrogen production from glycerol: water mixtures under solar light irradiation, Int. J. Hydrogen Energy 38 (2013) 9655–9664.
[39] D.P. Kumar, N.L. Reddy, M. Karthik, B. Neppolian, J. Madhavan, M.V. Shankar, Solar light sensitized p-Ag_2O/n-TiO_2 nanotubes heterojunction photocatalysts for enhanced hydrogen production in aqueous-glycerol solution, Sol. Energy Mater. Sol. Cells 154 (2016) 78–87.
[40] X. Fu, J. Long, X. Wang, D.Y.C. Leung, Z. Ding, L. Wu, Z. Zhang, Z. Li, X. Fu, Photocatalytic reforming of biomass: a systematic study of hydrogen evolution from glucose solution, Int. J. Hydrogen Energy 33 (2008) 6484–6491.
[41] J. Greaves, L. Al-Mazroai, A. Nuhu, P. Davies, M. Bowker, Photocatalytic methanol reforming on Au/TiO_2 for hydrogen production, Gold Bull. 39 (2006) 216–219.
[42] A.V. Puga, Photocatalytic production of hydrogen from biomass-derived feedstocks, Coord. Chem. Rev. 315 (2016) 1–66.
[43] M. Feilizadeh, G. Mul, M. Vossoughi, E. coli inactivation by visible light irradiation using a Fe–Cd/TiO_2 photocatalyst: statistical analysis and optimization of operating parameters, Appl. Catal. B: Environ. 168 (2015) 441–447.
[44] M. Antonopoulou, I. Konstantinou, Optimization and modeling of the photocatalytic degradation of the insect repellent DEET in aqueous TiO_2 suspensions, CLEAN–Soil Air Water 41 (2013) 593–600.

[45] M.M. Mohammadi, M. Vossoughi, M. Feilizadeh, D. Rashtchian, S. Moradi, I. Alemzadeh, Effects of electrophoretic deposition parameters on the photocatalytic activity of TiO_2 films: optimization by response surface methodology, Coll. Surf. A 452 (2014) 1–8.
[46] M. Feilizadeh, M. Rahimi, S.M. Zakeri, N. Mahinpey, M. Vossoughi, M. Qanbarzadeh, Individual and interaction effects of operating parameters on the photocatalytic degradation under visible light illumination: response surface methodological approach, Can. J. Chem. Eng. (2017), http://dx.doi.org/10.1002/cjce.22808, in press.
[47] A.R. Amani-Ghadim, M.S.S. Dorraji, Modeling of photocatalyatic process on synthesized ZnO nanoparticles: kinetic model development and artificial neural networks, Appl. Catal. B: Environ. 163 (2015) 539–546.
[48] B. Saha, P. Chowdhury, A.K. Ghoshal, Al-MCM-41 catalyzed decomposition of polypropylene and hybrid genetic algorithm for kinetics analysis, Appl. Catal. B: Environ. 83 (2008) 265–276.
[49] S.A.L. Bastos, P.A.L. Lopes, F.N. Santos, L.A. Silva, Experimental design as a tool to study the reaction parameters in hydrogen production from photoinduced reforming of glycerol over CdS photocatalyst, Int. J. Hydrogen Energy 39 (2014) 14588–14595.
[50] X.-Z. Ding, X.-H. Liu, Y.-Z. He, Grain size dependence of anatase-to-rutile structural transformation in gel-derived nanocrystalline titania powders, J. Mater. Sci. Lett. 15 (1996) 1789–1791.
[51] M. Feilizadeh, I. Alemzadeh, A. Delparish, M.R.K. Estahbanati, M. Soleimani, Y. Jangjou, A. Vosoughi, Optimization of operating parameters for efficient photocatalytic inactivation of Escherichia coli based on a statistical design of experiments, Water Sci. Technol. 71 (2015) 823–831.
[52] A. Pasini, Artificial neural networks for small dataset analysis, J. Thorac. Dis. 7 (2015) 953–960.
[53] M. Zarei, A.R. Khataee, R. Ordikhani-Seyedlar, M. Fathinia, Photoelectro-Fenton combined with photocatalytic process for degradation of an azo dye using supported TiO_2 nanoparticles and carbon nanotube cathode: neural network modeling, Electrochim. Acta 55 (2010) 7259–7265.
[54] D.G. Garson, Interpreting Neural Network Connection Weights, 6, AI Expert, 1991, pp. 46–51.
[55] A.R. Khataee, O. Mirzajani, UV/peroxydisulfate oxidation of CI Basic Blue 3: modeling of key factors by artificial neural network, Desalination 251 (2010) 64–69.
[56] M.A. Shah, Growth of uniform nanoparticles of platinum by an economical approach at relatively low temperature, Scientia Iranica 19 (2012) 964–966.
[57] C. Montero-Ocampo, J.R. Vargas Garcia, E. Arce Estrada, Comparison of TiO_2 and TiO_2-CNT as cathode catalyst supports for ORR, Int. J. Electrochem. Sci. 8 (2013) 12780–12800.
[58] J.W. Niemantsverdriet, Spectroscopy in Catalysis: An Introduction, John Wiley & Sons, 2007.
[59] C.R. López, E.P. Melián, J.A. Ortega Méndez, D.E. Santiago, J.M. Doña Rodríguez, O. González Díaz, Comparative study of alcohols as sacrificial agents in H_2 production by heterogeneous photocatalysis using Pt/TiO_2 catalysts, J. Photochem. Photobiol. A: Chem. 312 (2015) 45–54.
[60] S. Moradi, M. Vossoughi, M. Feilizadeh, S.M.E. Zakeri, M.M. Mohammadi, D. Rashtchian, A.Y. Booshehri, Photocatalytic degradation of dibenzothiophene using La/PEG-modified TiO_2 under visible light irradiation, Res. Chem. Intermed. 41 (2015) 4151–4167.
[61] V.A. Sakkas, M.A. Islam, C. Stalikas, T.A. Albanis, Photocatalytic degradation using design of experiments: a review and example of the Congo red degradation, J. Hazard. Mater. 175 (2010) 33–44.
[62] A. Speltini, M. Sturini, D. Dondi, E. Annovazzi, F. Maraschi, V. Caratto, A. Profumo, A. Buttafava, Sunlight-promoted photocatalytic hydrogen gas evolution from water-suspended cellulose: a systematic study, Photochem. Photobiol. Sci. 13 (2014) 1410–1419.
[63] A. Speltini, M. Sturini, F. Maraschi, D. Dondi, A. Serra, A. Profumo, A. Buttafava, A. Albini, Swine sewage as sacrificial biomass for photocatalytic hydrogen gas production: explorative study, Int. J. Hydrogen Energy 39 (2014) 11433–11440.
[64] L.S. Al-Mazroai, M. Bowker, P. Davies, A. Dickinson, J. Greaves, D. James, L. Millard, The photocatalytic reforming of methanol, Catal. Today 122 (2007) 46–50.
[65] T. Sreethawong, T. Puangpetch, S. Chavadej, S. Yoshikawa, Quantifying influence of operational parameters on photocatalytic H_2 evolution over Pt-loaded nanocrystalline mesoporous TiO_2 prepared by single-step sol–gel process with surfactant template, J. Power Sources 165 (2007) 861–869.
[66] A. Yamakata, T.-a. Ishibashi, H. Onishi, Kinetics of the photocatalytic water-splitting reaction on TiO_2 and Pt/TiO_2 studied by time-resolved infrared absorption spectroscopy, J. Mol. Catal. A: Chem. 199 (2003) 85–94.
[67] E.P. Melián, C.R. López, A.O. Méndez, O.G. Díaz, M.N. Suárez, J.M.D. Rodríguez, J.A. Navío, D.F. Hevia, Hydrogen production using Pt-loaded TiO_2 photocatalysts, Int. J. Hydrogen Energy 38 (2013) 11737–11748.
[68] C. Kormann, D.W. Bahnemann, M.R. Hoffmann, Photolysis of chloroform and other organic molecules in aqueous titanium dioxide suspensions, Environ. Sci. Technol. 25 (1991) 494–500.
[69] M.H. Habibi, A. Hassanzadeh, S. Mahdavi, The effect of operational parameters on the photocatalytic degradation of three textile azo dyes in aqueous TiO_2 suspensions, J. Photochem. Photobiol. A: Chem. 172 (2005) 89–96.
[70] S. Jacob, R. Banerjee, Modeling and optimization of anaerobic codigestion of potato waste and aquatic weed by response surface methodology and artificial neural network coupled genetic algorithm, Bioresour. Technol. 214 (2016) 386–395.